Arabidopsis thaliana expresses two functional isoforms of Arvp, a protein involved in the regulation of cellular lipid homeostasis ☆

Oriol Forés [a], Montserrat Arró [a], Albert Pahissa [a], Sergi Ferrero [b], Melody Germann [c], Joseph Stukey [d], Virginia McDonough [d], Joseph T. Nickels Jr. [c], Narciso Campos [b], Albert Ferrer [a,*]

[a] *Departament de Bioquímica i Biologia Molecular, Facultat de Farmàcia, Universitat de Barcelona, Avda. Diagonal 643, Barcelona-08028, Spain*
[b] *Departament de Bioquímica i Biologia Molecular, Facultat de Biologia, Universitat de Barcelona, Barcelona-08028, Spain*
[c] *Department of Biochemistry and Molecular Biology, Drexel University, College of Medicine, Philadelphia, PA 19102, USA*
[d] *Department of Biology, Hope College, Holland, MI 49422, USA*

Abstract

Arv1p is involved in the regulation of cellular lipid homeostasis in the yeast *Saccharomyces cerevisiae*. Here, we report the characterization of the two *Arabidopsis thaliana ARV* genes and the encoded proteins, AtArv1p and AtArv2p. The functional identity of AtArv1p and AtArv2p was demonstrated by complementation of the thermosensitive phenotype of the *arv1*Δ yeast mutant strain YJN1756. Both *A. thaliana* proteins contain the bipartite Arv1 homology domain (AHD), which consists of an NH_2-terminal cysteine-rich subdomain with a putative zinc-binding motif followed by a C-terminal subdomain of 33 amino acids. Removal of the cysteine-rich subdomain has no effect on Arvp activity, whereas the presence of the C-terminal subdomain of the AHD is critical for Arvp function. Localization experiments of AtArv1p and AtArv2p tagged with green fluorescent protein (GFP) and expressed in onion epidermal cells demonstrated that both proteins are exclusively targeted to the endoplasmic reticulum. Analysis of β-glucuronidase (GUS) activity in transgenic *A. thaliana* plants carrying chimeric *ARV1*::*GUS* and *ARV2*:: *GUS* genes showed that *ARV* gene promoters direct largely overlapping patterns of expression that are restricted to tissues in which cells are actively dividing or expanding. The results of this study support the notion that plants, yeast and mammals share common molecular mechanisms regulating intracellular lipid homeostasis.

Keywords: Arabidopsis; Lipid homeostasis; Sterol; Sphingolipid; Plant; Yeast

1. Introduction

The mechanisms regulating lipid homeostasis in eukaryotes and in particular those involved in intracellular lipid trafficking are still poorly understood at the molecular level. Nevertheless, a number of studies in animal and yeast cells support the existence of a coordinated regulation between sphingolipid biosynthesis and sterol metabolism [1–4]. Recently, the *Saccharomyces cerevisiae ARV1* gene was isolated in a genetic screen designed to identify genes that are essential for viability when yeast cells are impaired in sterol esterification [5]. The encoded Arv1p contains a novel NH_2-terminal domain, defined as the Arv1 homology domain (AHD), which includes a putative zinc-binding motif. Arv1p is predicted to have six transmembrane domains [5] and has been found to localize in the endoplasmic reticulum (ER) or the Golgi apparatus of yeast

Abbreviations: AHD, Arv1 homology domain; CaMV, cauliflower mosaic virus; DsRed, Discosoma red fluorescent protein; ER, endoplasmic reticulum; HA, peptide from human hemagglutinin; GPD, glyceraldehyde phosphate dehydrogenase; GFP, green fluorescent protein; GUS, β-glucuronidase; UBQ, polyubiquitin; IPC, inositolphosphorylceramide; MIPC, mannose inositolphosphorylceramide; MIP_2C, mannose diinositolphosphorylceramide; RT, reverse transcriptase; T3RE, ER-targeted variant of DsRed; X-Gluc, 5-bromo-4-chloro-3-indolyl-β-D-glucuronide; YNB, yeast nitrogen base

☆ The nucleotide sequence data for *A. thaliana* ARV1 and ARV2 cDNAs have been submitted to GenBank Database under the accession numbers AY758070 and AY758071, respectively.

* Corresponding author. Tel.: +34 934034497; fax: +34 934024520.
E-*mail address:* albertferrer@ub.edu (A. Ferrer).

cells in a bud size- and/or growth phase-dependent manner, suggesting a possible cell-cycle regulated localization [6]. Deletion of *ARV1* leads to altered levels and distribution of intracellular sterols. The overall content of free sterols increases by about 50% and that of steryl esters by about 75%. Moreover, sterol concentration decreases in plasma membrane whereas elevated sterol levels are observed in ER and vacuolar membranes. Based on these results, a role for Arv1p in sterol trafficking has been proposed [5]. The finding that Arv1p interacts directly with Erg11p, the enzyme that demethylates lanosterol in the course of ergosterol biosynthesis, further substantiates the relationship between Arv1p and sterol metabolism in yeast [7]. Studies from Swain et al. [6] have shown that *arv1*Δ mutant yeast cells also display defects in their ability to properly synthesize and maintain sphingolipid levels. Mutant cells have reduced rates of biosynthesis and lower steady-state levels of complex sphingolipids while accumulating certain ceramide species. In line with these results, mutations in *ARV1* have also been isolated in a genetic screen designed to obtain yeast mutants with defects in sphingolipid metabolism [6]. These observations have led to propose that Arv1p either may primarily regulate sphingolipid metabolism, such that altered sterol levels and distribution might result from improper sphingolipid homeostasis, or act as a common dual regulator of both sphingolipid and sterol metabolism and transport [6]. A human Arv1p has also been cloned and shown to replace yeast Arv1p function completely in regulating yeast sterol and sphingolipid metabolism [5,6].

In regards to plants, far less attention has been paid to the mechanisms involved in the maintenance of cellular lipid homeostasis. In fact, one of the fundamental questions still to be addressed is how intracellular lipid homeostasis is maintained in plant cells and which mechanisms regulate cross-talk between the metabolism of different lipid species [8,9]. Some recent findings support the view that sterol and sphingolipid metabolism are also coordinately regulated in plants. Studies using leek seedlings have shown that inhibition of the sterol biosynthetic pathway also impairs phosphatidylserine and glucosylceramide synthesis [10]. More recently, plasma membranes of plant cells have been shown to contain lipid rafts [11,12], which are discrete microdomains of membranes enriched in sphingolipids and sterols previously identified and characterized in animal and yeast cells [13–15]. To gain insight into the mechanisms regulating lipid homeostasis in plant cells, we undertook the present study focusing on the functional characterization of the two *Arabidopsis thaliana ARV* genes and the encoded proteins.

2. Materials and methods

2.1. Plant materials and yeast strains

A. thaliana plants (var. Columbia 3) were grown either on soil irrigated with mineral nutrients [16] at 22 °C under a 8 h light/16 h dark illumination regime with 130 μmol photons m^{-2} s^{-1} "daylight" fluorescent illumination or axenically in Petri dishes containing solid (0.8% w/v agar) germination medium (GM; Murashige and Skoog medium (ICN Biomedicals) supplemented with 0.5 g l^{-1} MES pH 5.7) under the same light and temperature conditions. Suspension-cultured *A. thaliana* T87 cells were grown as described [17]. Yeast mutant strain YJN1756 (*MAT*α *arv1::KAN*, *ade2*, *his3*, *leu2*, *trp1*, *ura3*) used in this study is derived from strain W303-1A [3]. The yeast strains were grown in either YPD [1% (w/v) yeast extract, 1% (w/v) bactopeptone, and 2% (w/v) glucose] or minimal medium [0.16% (w/v) YNB (yeast nitrogen base) without amino acids and without $(NH_4)_2SO_4$, 0.5% (w/v) $(NH_4)_2SO_4$, and 2% (w/v) glucose] supplemented with the appropriate amino acids and adenine.

2.2. Cloning of ARV1 and ARV2 cDNA sequences

A first-strand cDNA pool was synthesized by reverse transcription of 2.5 μg total RNA from axenically grown 10-day-old *A. thaliana* seedlings with an oligo (dT) primer (5′-GCGTCGACTGCAGGGCTTTTTTTTTTTTTTTT-3′). The cDNA mixture was used as template for independent PCR reactions using primer pairs ARV1-f1 and ARV1-r1 for the amplification of ARV1 cDNA, and ARV2-f1 and ARV2-r1 for the amplification of ARV2 cDNA. The *A. thaliana* genomic sequence AC007323 (GenBank) was used to design primers ARV1-f1 (5′-CGGGATTCAGACCCGGACTCTAATTGCT-3′; reverse complement of bp 8420 to 8439) and ARV1-r1 (5′-CGGTCGACCTGGAAGCTGATGGGATCATAC-3′, bp 6601 to 6622), and the *A. thaliana* genomic sequence AL161492 (GenBank) was used to design primers ARV2-f1 (5′-CGGGATCCCAACAGTCACAGACACAGAG-3′; bp 65298 to 65317) and ARV2-r1, (5′-CGGTCGACCACAAGTTCCTTGCAAGAGAAG-3′; reverse complement of bp 66757 to 66778). *Bam*HI and *Sal*I restriction sites (underlined) were added at the 5′ end of the forward and reverse primers, respectively. The amplified cDNAs were cloned into pGemT-Easy (Promega), yielding plasmids pGTARV1 and pGTARV2.

2.3. Construction of yeast expression vectors and functional complementation of a S. cerevisiae ARV1 null mutant

The ARV1 and ARV2 cDNA fragments were excised as *Bam*HI–*Sal*I fragments from pGTARV1 and pGTARV2 and cloned into the corresponding sites of the yeast expression vector pJR1133, which is identical to pJR1138 [18] except for containing the *URA3* marker instead of *LEU2*. The resulting plasmids, pJRAtArv1p and pJRAtArv2p, carried the cDNA fragments under the control of the yeast glyceraldehyde phosphate dehydrogenase (GPD) gene promoter. To construct plasmids pJRAtArv2p-HA, pJRAtArv2pΔ35-HA, pJRAtArv2pΔ46-HA, pJRAtArv2pΔ56-HA and pJRAtArv2pΔ68-HA, the corresponding cDNA fragments were amplified by PCR using as forward primer either ARV2-f1, ARV2Δ35 (5′-GGATCC**ATG**GAAGAAGTAGCAGAC-3′), ARV2Δ46 (5′-GGATCC**ATG**CTATTGATTATTTTATC-3′), ARV2Δ56 (5′-GGATCC**ATG**-CACAAAACAAAGGCT-3′) or ARV2Δ68 (5′-GGATCC**ATG**GTTGTTAATCAAGAA-3′), a common reverse primer ARV2-HA-r (5′-GTCGAC**TCA***CGCATAGTCAGGAACATCGTATGGGTA*TACGATTCTGAAAAAATAAGACATATA-3′), and pGTARV2 as template. *Bam*HI and *Sal*I restriction sites (underlined) were added at the 5′ end of the forward and reverse primers, respectively. Translational start and stop codons are shown in bold. The sequence coding for the hemagglutinin (HA) epitope (YPYDVPDYA) is shown in italics. The PCR products were cloned into pGemT-Easy, excised as *Bam*HI/*Sal*I fragments, and cloned into the corresponding sites of pJR1133. To create pAtArv2p4Ser-HA, the amino acid substitutions Cys^8Ser, Cys^{11}Ser, Cys^{32}Ser, and Cys^{35}Ser were introduced by a PCR-based overlap extension method [19]. To generate substitutions Cys^{32}Ser and Cys^{35}Ser, independent PCR reactions were carried out using pGTARV2 as template and either primer pair ARV2-f1 and ARV2-C32/35S-r (5′-TACTTCTTCGC-**T**ATTCTCGC**T**TTTCATGAG-3′) or primer pair ARV2-C32/35S-f (5′-CTCATGAAA**A**GCGAGAAT**A**GCGAAGAAGTA-3′) and ARV2-C-r (5′-GCAAGCTTCTATAAGTATCTAGAAG-3′). Nucleotide changes to introduce cysteine to serine substitutions are shown in bold. Primer ARV2-C-r contains a *Hin*dIII restriction site (underlined). About 200 ng of each PCR product were mixed and used as template in the subsequent PCR-based overlap extension reaction, which was carried out using primers ARV2-f1 and ARV2-C-r. The resulting fragment was cloned into pGemT-Easy yielding clone pGTC32/35S. Substitutions Cys^8Ser and Cys^{11}Ser were introduced using pGTC32/35S as template and either primer pair ARV2-f1 and ARV2-C8/11S-r (5′-CTTGTGCCCAC**T**CTCTACAC**T**CGTCTTCTT-3′) or primer pair ARV2-

C8/11S-f (5′-AAGAAGACG**A**GTGTAGAG**A**GTGGGCACAAG-3′) and ARV2-C-r. Nucleotide changes to introduce cysteine to serine substitutions are shown in bold. The amplified products were used as template in a PCR-based overlap extension reaction carried out as described above. The PCR product was cloned into pGemT-Easy, yielding clone pGTC8/11/32/35S, from which it was excised as a *Bam*HI–*Hin*dIII fragment to replace the equivalent cDNA fragment in pGTARV2-HA, yielding clone pGTAtArv2p4-Ser-HA. The mutagenized cDNA was then excised as a *Bam*HI/*Sal*I fragment and cloned into the corresponding sites of pJR1133, yielding clone pJRAtArv2p4Ser-HA. Strain YJN1756 was transformed with pJR1133 and the pJR1133-derived plasmids by the lithium acetate procedure [20]. Ura^+ transformants were selected at 27 °C on agar plates containing minimal medium. Selected Ura^+ colonies were streaked on agar plates containing YPD and incubated at either 27 or 37 °C. For growth complementation tests in liquid media, single colonies of recombinant YJN1756 strains grown for 2 days on agar plates containing minimal medium were picked and cultured at 27 °C in minimal medium until an OD_{600} of 1.5. Cells were then diluted into YPD (OD_{600}=0.05–0.1) and growth at 37 °C monitored by measuring the absorbance at 600 nm. Lipid analyses were carried out as described [6].

2.4. Preparation of yeast protein extracts, gel electrophoresis, and immunoblotting

Recombinant YJN1756 strains were grown at 27 °C in liquid minimal medium to an OD_{600} of 0.8 and total protein extracts were prepared as previously described [21]. Aliquots of supernatant were fractionated in SDS-PAGE gels and transferred to Hybond-P membranes (Amersham) according to standard protocols. Western blot analysis was performed using anti-HA antibodies (1:200 dilution; Santa Cruz Biotechnology, Santa Cruz, CA) and horseradish peroxidase-conjugated anti-rabbit IgG (1:5.000 dilution; Amersham).

2.5. Construction of plasmids for the expression of GFP-AtArv1p, GFP-AtArv2p, and GFP-AtArv2pΔ68 in onion epidermal cells

The sequence coding for AtArv1p was amplified by PCR using forward primer ARV1-f2 (5′-CGAGCTC**ATG**GCGGCGAGTGAA-3′), reverse primer ARV1-r2 (5′-CGGGATCCTGGAAGCTGATGGGA-3′), and pGTARV1 as template. The sequences coding for AtArv2p and AtArv2pΔ68 were amplified using as forward primer either ARV2-f2 (5′-CGAGCTC**ATG**GCGAGAGA-GAAG-3′) or ARV2Δ68-f2 (5′-CGAGCTCATGG TTGTTAATCAAGAA-3′), reverse primer ARV2-r2 (5′-CGGGATCCCCTTGCA AGAGAAGA-3′), and pGTARV2 as template. Translational start codons are shown in bold. *Sac*I and *Bam*HI restriction sites (underlined) were added at the 5′ end of the forward and reverse primers, respectively. The amplified fragments were digested with *Sac*I and *Bam*HI, and cloned in frame with the green fluorescent protein (GFP) coding sequence into the corresponding sites of pGFP-MRC [18], yielding plasmids pGFP-AtArv1p, pGFP-AtArv2p, and pGFP-AtArv2pΔ68, which carried the chimeric genes under the transcriptional control of the cauliflower mosaic virus (CaMV) 35S gene promoter. To obtain a variant of the *Discosoma* red fluorescent protein (DsRed) targeted to the ER, we followed the rationale that had proven successful with GFP [22]. The DsRed.T3 coding sequence [23] was modified by inserting a sequence encoding the same chitinase transit peptide at the start codon and a sequence encoding the KDEL ER-retention signal [24] at the stop codon. The resulting coding sequence was used to replace the GFP sequence in plasmid pRTL2-sGFP [25] to yield plasmid pT3RE. All constructs were sequenced to confirm the in-frame fusions. GFP-AtArvp and T3RE fusion plasmids were introduced into onion epidermal cells by micro-bombardment using tungsten particles coated with plasmid DNA and a Biolistic PDS-1000/He system (Bio-Rad) with a 1100 psi rupture disc (Bio-Rad). Onion pieces were kept in darkness at 22 °C for 16 h and epidermal cells were examined by laser confocal-scanning fluorescence microscopy (Olympus IX70). Green fluorescence was detected using a BP515–525 filter after excitation with blue light at 488 nm, and red fluorescence was detected using a BA560F filter after excitation with green light at 543 nm.

2.6. RT-PCR expression analysis

Total RNA was extracted using the RNEasy® Plant Mini Kit (QIAGEN Sciences) from T87 cells collected at the mid-exponential growth phase and different tissues of *A. thaliana* plants according to the manufacturer's instructions. Reverse transcriptase reactions were carried out using 1 μg of total RNA and Transcriptor Reverse Transcriptase (Roche Diagnostics GmbH) according to standard protocols. PCR reactions were carried out by 32 cycles of amplification (45 s at 95 °C, 60 s at 57 °C and 90 s at 72 °C) and a 5 min final extension at 72 °C, using as template 2 μl of the single-stranded cDNA pools and the PureTaq Ready-To-Go PCR beads (Amersham Biosciences). Primer pairs RTARV1-f (5′-GGTGTCTTATCTGCAAACGCTG-3′) and RTARV1-r (5′-GAAGCTGATGGGATCATAC-3′), and RTARV2-f (5′-CGGAT-CAAATGTGTCTATGAGC-3′) and RTARV2-r (5′-GTTCCTTGCAAGA-GAAG-3′) were used for expression analysis of *ARV1* and *ARV2*, respectively. The expression of the *A. thaliana* polyubiquitin (*UBQ*) 10 gene (At4g05320) was analyzed using primers UBQ-f (5′-GGACCAGCAGCGTCTCATCTTCGC-3′) and UBQ-r (5′-CTTATTCATCAGGGATTATACAAG-3′).

2.7. Construction of ARV::GUS gene fusions and generation of transgenic plants

To construct the *ARV1::GUS* gene fusion, a 1574 bp fragment from the 5′-region of the *ARV1* gene was amplified by PCR using forward primer ARV1-GUS-f (5′-GTCTAGAGATCGGATATGACATAGCGGA-3′; bp −1547 to −1527 in the *ARV1* gene), reverse primer ARV1-GUS-r (5′-GCGGTACC-CACGCATCTGTGTTCACTC-3′; complementary to bp +9 to +27 with respect to the first base of the ATG codon of *ARV1*), and genomic *A. thaliana* DNA as template. For the *ARV2::GUS* gene fusion, a 1534 bp fragment from the 5′-region of the *ARV2* gene was amplified by PCR using forward primer ARV2-GUS-f (5′-GTCTAGACTTCTCTCTCGCCATCTC-3′; bp −1519 to −1501 in the *ARV2* gene), reverse primer ARV2-GUS-r (5′-GCGGTACCTGCCTTCTG-TAGCTAAGCTG-3′; complementary to bp −3 to +15 with respect to the ATG codon of the *ARV2*), and genomic *A. thaliana* DNA as template. *Xba*I and *Kpn*I restriction sites (underlined) were added at the 5′ end of the forward and reverse primers, respectively. The PCR fragments were digested with *Xba*I and *Kpn*I, and cloned into the corresponding sites of binary vector pBI121 (Clontech), yielding plasmids pBIARV1::GUS and pBIARV2::GUS, respectively. Fusions between *ARV1* and *ARV2* 5′-regions and the GUS-coding sequence were confirmed by sequencing. *A. thaliana* plants were transformed using the in-planta infiltration method [26] and *Agrobacterium tumefaciens*, strain C58C1 (pGV2260), harbouring pBIARV1::GUS and pBIARV2::GUS. Seeds from infiltrated plants were surface sterilized and sown in Petri dishes containing GM supplemented with 50 μg ml^{-1} kanamycin. Kanamycin-resistant seedlings (T_1) were transplanted into soil and grown to maturity. Histochemical analysis of GUS activity was performed as previously described [27].

3. Results

3.1. Cloning and sequence analysis of two A. thaliana ARV cDNAs

Using the amino acid sequence of a putative *A. thaliana* Arvp (Accession Number CAB77721) [5] as query, we identified two *A. thaliana* genomic sequences (At4g01510 and At1g01020) that might encode Arv1p-like proteins. The At4g01510 gene was predicted to contain 9 exons that encoded the sequence of 252 amino acids used as query in the data-base search whereas the At1g01020 gene was predicted to consist of 5 exons that encoded a polypeptide of 128 amino acids. An additional search in the TAIR plant protein data-base allowed us to identify a protein of 245 amino acids (Accession Number AAF26477), which matched the first 118 residues of the protein potentially encoded by At1g01020. A detailed analysis of the

sequence downstream of the putative exon 5 of At1g01020 suggested that it might contain 4 additional exons, since conceptual translation of these 9 putative exons gave rise to an amino acid sequence identical to that of entry AAF26477. To define the true organization of the predicted *ARV* genes and to demonstrate their functionality, cDNA sequences encompassing their complete coding region were isolated by RT-PCR and RNA from 10-day-old *A. thaliana* seedlings. A cDNA fragment of 825-bp (GenBank Accession Number AY758070) with a sequence identical to that of the 9 putative exons of At1g01020 (hereafter referred to as *ARV1* gene) was amplified using primers located upstream (ARV1-f1) and downstream (ARV-r1) of the predicted translational start and stop codons, respectively, of *ARV1*. However, all attempts to amplify a cDNA corresponding to At4g01510 using different forward primers located upstream of the predicted ATG start codon, a reverse primer located downstream the coding region (ARV2-r1), and RNA from different tissues of *A. thaliana* repeatedly failed. Additional RT-PCR experiments were carried out using a new forward primer (ARV2-f1) located between the 5′-most ATG codon and an in-frame internal ATG codon and reverse primer ARV2-r1. Using this pair of primers, we amplified a cDNA of 732 bp (GenBank Accession Number AY758071) with a sequence identical to that of the 9 predicted exons of At4g01510 (hereafter referred to as *ARV2* gene). Conceptual translation of the cloned cDNAs revealed that the encoded proteins, further referred to as AtArv1p and AtArv2p, consist of 245 and 228 amino acids, respectively, (Fig. 1) instead of the 128 and 252 amino acids initially assigned to these proteins. AtArv1p and AtArv2p share 66% overall identity and are 14% and 17% identical to *S. cerevisiae* Arv1p, and 20% and 33% identical to human Arv1p, respectively (Fig. 1). Interestingly, the NH_2-terminal region of these proteins shows a much higher level of identity than the rest of the protein. Indeed, 15 out of the 18 amino acid residues conserved in all four proteins are found in the first 68 amino acids that form the AHD. This domain consists of two well-defined subdomains: a NH_2-terminal cysteine-rich subdomain, which differs in length depending on the organism but always includes a block of 28 amino acids with the signature of a zinc-binding motif ($Cys–X_2–Cys–X_{20}–Cys–X_2–Cys$; positions 8 to 35 in AtArv proteins), and a C-terminal subdomain of 33 residues (positions 36 to 68 in AtArv proteins) (Fig. 1).

3.2. A. thaliana Arv proteins complement a S. cerevisiae ARV1 null mutant

To evaluate the functionality of AtArv1p and AtArv2p, the corresponding cDNA sequences were expressed in the yeast mutant strain YJN1756. This strain bears a disruption of the *ARV1* gene that renders cells thermosensitive, such that *arv1*Δ cells can grow at 27 °C (permissive temperature) but not at 37 °C (restrictive temperature) [6]. Strain YJN1756 was transformed with plasmids pJRAtArv1p, pJRAtArv2p and

Fig. 1. Alignment of the Arv proteins from *A. thaliana*, *H. sapiens*, and *S. cerevisiae*. Residues conserved in all four sequences are shown in black boxes whereas those conserved in three out of the four sequences are shown in grey boxes. Hyphens indicate gaps introduced to optimize the alignment. Amino acid residues are numbered on the right. The sequence with the signature of a zinc-binding motif is underlined while cysteine residues in this sequence are denoted by asterisks. The sequences shown have the following GenBank accession numbers: *Arabidopsis thaliana* Arv1p AAV92715, *Arabidopsis thaliana* Arv2p AAV92716, *Homo sapiens* AAG47671.1, and *Saccharomyces cerevisiae* AAB67397.

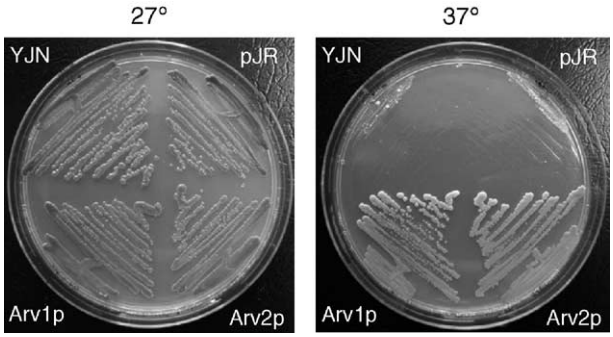

Fig. 2. Functional complementation of the *S. cerevisiae ARV1* null mutant strain YJN1756 by overexpression of AtArv1p and AtArv2p. Cells of strain YJN1756 and of the same strain transformed with plasmids pJR1133, pJRARV1 and pJRARV2 were streaked onto YPD plates and incubated at 27 and 37 °C for three and 2 days, respectively.

pJR1133, and the resulting recombinant YJN1756 cells were tested for their ability to grow at the permissive and restrictive temperatures. As is shown in Fig. 2, overexpression of AtArv1p and AtArv2p restored the viability of *arv1*Δ cells at the restrictive temperature whereas neither *arv1*Δ cells nor *arv1*Δ cells harbouring pJR1133 could grow at this temperature. These results demonstrate that AtArv1p and AtArv2p can both substitute for yeast Arv1p.

3.3. Overexpression of A. thaliana AtArv2p suppresses the lipid metabolic defects of a S. cerevisiae ARV1 null mutant

To check whether the observed functional complementation of the yeast *ARV1* null mutant by *A. thaliana* Arv proteins was due to the restoration of normal sterol and sphingolipid metabolism, levels of individual sterols were determined by GC/MS in wild-type yeast cells, *arv1*Δ cells and *arv1*Δ cells overexpressing AtArv2p grown at the permissive and restrictive temperatures. Cells overexpressing AtArv2p accumulated higher levels of ergosterol, the major yeast sterol end-product, than mutant cells at either growth temperature analyzed (Fig. 3A and B). In *arv1*Δ cells overexpressing AtArv2p grown at 27 °C ergosterol accounted for approximately 65% of total sterol content, whereas in *arv1*Δ and wild-type cells, it represented approximately 55% and 71% of total sterols, respectively (Fig. 3A). At 37 °C, ergosterol accounted for approximately 53% of total sterol content in *arv1*Δ cells overexpressing AtArv2p, whereas it accounted for approximately 48% and 59% of total sterols in *arv1*Δ and wild type cells, respectively (Fig. 3B). Furthermore, at both growth temperatures overexpression of AtArv2p restored wild-type levels of sterol biosynthetic intermediates to *arv1*Δ cells, including those of several unknown intermediates.

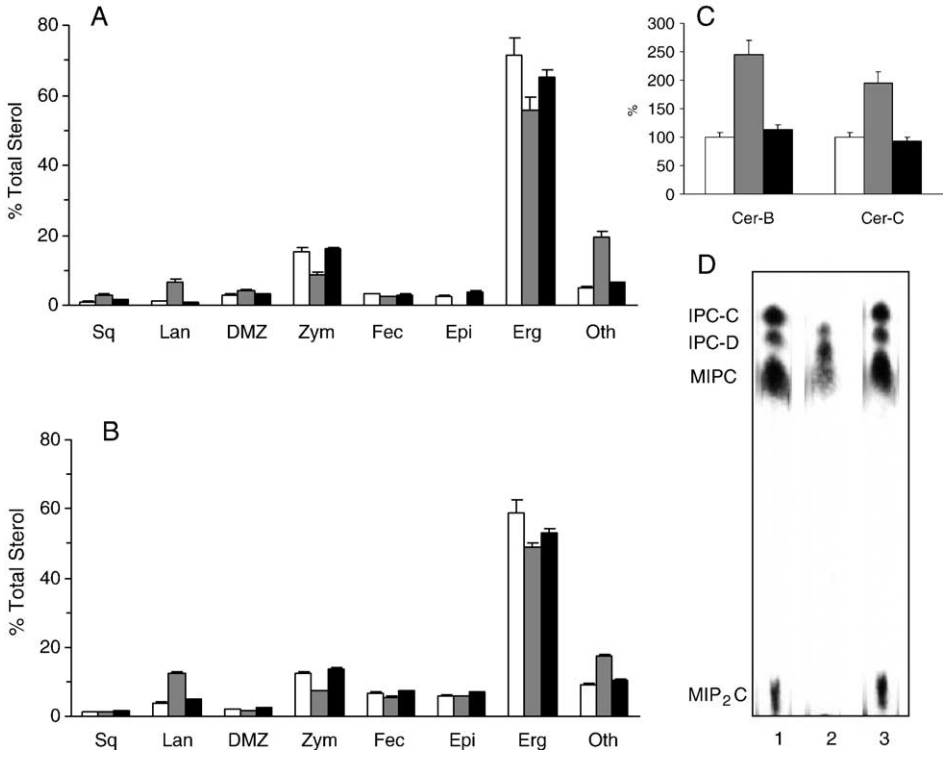

Fig. 3. Overexpression of AtArv2p restores normal sterol and sphingolipid metabolism to yeast *arv1*Δ cells. The levels of individual sterols in wild-type (white bars), *arv1*Δ (grey bars) and *arv1*Δ cells overexpressing AtArv2p (black bars) were determined at 27 °C (A) and 37 °C (B) using GC/MS analysis. Sq, squalene; Lan, lanosterol; DMZ, dimethylzymosterol; Zym, zymosterol; Fec, fecosterol; Epi, episterol; Erg, ergosterol; Oth, novel sterol intermediates. Levels of individual sterols are represented as % of total sterol contents. (C) Ceramide-B (Cer-B) and ceramide-C (Cer-C) levels in wild-type (white bars), *arv1*Δ (grey bars) and *arv1*Δ cells overexpressing AtArv2p (black bars). Cells were steady-state radiolabeled with [^{3}H]dihydrosphingosine at 37 °C and the ceramides were extracted and analyzed as described in Materials and methods. Wild type ceramide-B and ceramide-C levels were given a value of 100%. The % values are the average of three independent experiments. (D) Sphingolipid biosynthesis. Wild-type (1), *arv1*Δ (2) and *arv1*Δ cells overexpressing AtArv2p (3) were steady-state radiolabeled with [^{3}H]inositol at 37 °C and the sphingolipids were extracted, deacylated, and resolved as described in Materials and methods.

To investigate whether AtArv2p was capable of replacing yeast Arv1p function in sphingolipid metabolism, we first examined the effects of AtArv2p overexpression on the steady-state levels of ceramides, the precursors of all complex yeast sphingolipids. Although yeasts contain a mixture of five ceramide forms, namely ceramide-A, -B, -B′, -C, and -D, we only measured the levels of forms B and C as these are the only ceramides whose levels are increased in *arv1*Δ cells [6]. As shown in Fig. 3C, overexpression of AtArv2p restored wild-type levels of ceramide-B and ceramide-C to *arv1*Δ cells. We next investigated whether overexpression of AtArv2p could restore sphingolipid biosynthesis to *arv1*Δ cells, which is severely impaired at the non-permissive growth temperature [6]. To this end, wild type cells, *arv1*Δ cells, and *arv1*Δ cells overexpressing AtArv2p were radiolabeled with [^{3}H]inositol and the rates of biosynthesis of sphingolipids were analyzed by TLC. As is shown in Fig. 3D, overexpression of AtArv2p restored sphingolipid biosynthesis to *arv1*Δ cells, since biosynthetic rates of inositolphosphorylceramide (IPC) species IPC-C, IPC-D, mannose inositolphosphorylceramide (MIPC) and mannose diinositolphosphorylceramide (MIP_2C) in *arv1*Δ cells overexpressing AtArv2p were identical to those in wild-type cells. Overexpression of AtArv2p also led to normal levels of phosphatidylglycerol (results not shown), the phospholipid that accumulates to a greater extent in *arv1*Δ cells [6]. Collectively, these results demonstrate that the ability of AtArv2p to restore the growth to *arv1*Δ cells at 37 °C is actually due to its ability to suppress the lipid metabolic defects of *arv1*Δ cells, thereby replacing yeast Arv1p function as a regulator of cellular lipid homeostasis. Given the high level of sequence identity between AtArv1p and AtArv2p, as well as the fact that AtArv1p also restored the viability of *arv1*Δ cells at 37 °C, we conclude that these proteins are the true *A. thaliana* orthologs of yeast and human Arv1p.

3.4. Functional analysis of the NH_2-terminal region of A. thaliana AtArv2p

To investigate whether the two subdomains of AHD are required for Arvp function, a series of AtArv2p NH_2-terminal nested deletion mutants (AtArv2pΔ35-HA, AtArv2pΔ46-HA, AtArv2pΔ56-HA, and AtArv2pΔ68-HA) and an AtArv2p mutant in which the four cysteine residues at positions 8, 11, 32, and 35 potentially involved in forming a zinc-binding motif (Fig. 1) were simultaneously replaced by serines (AtArv2p4Ser-HA), were assayed for their ability to restore growth of *arv1*Δ cells at 37 °C on solid and in liquid media (Fig. 4). An HA epitope was added at the C terminus of the wild-type and mutant proteins to determine the effects of the mutations on the levels of the expressed proteins (Fig. 4C). As is shown in Fig. 4 A and B, the presence of the HA tag did not affect the capacity of AtArv2p-HA to restore the growth of *arv1*Δ cells at 37 °C. Interestingly, the growth of *arv1*Δ cells overexpressing AtArv2pΔ35-HA at 37 °C was comparable to that of cells overexpressing AtArv2p-HA whereas *arv1*Δ cells overexpressing AtArv2pΔ46-HA, AtArv2pΔ56-HA and AtArv2pΔ68-HA were unable to grow at the restrictive temperature either on

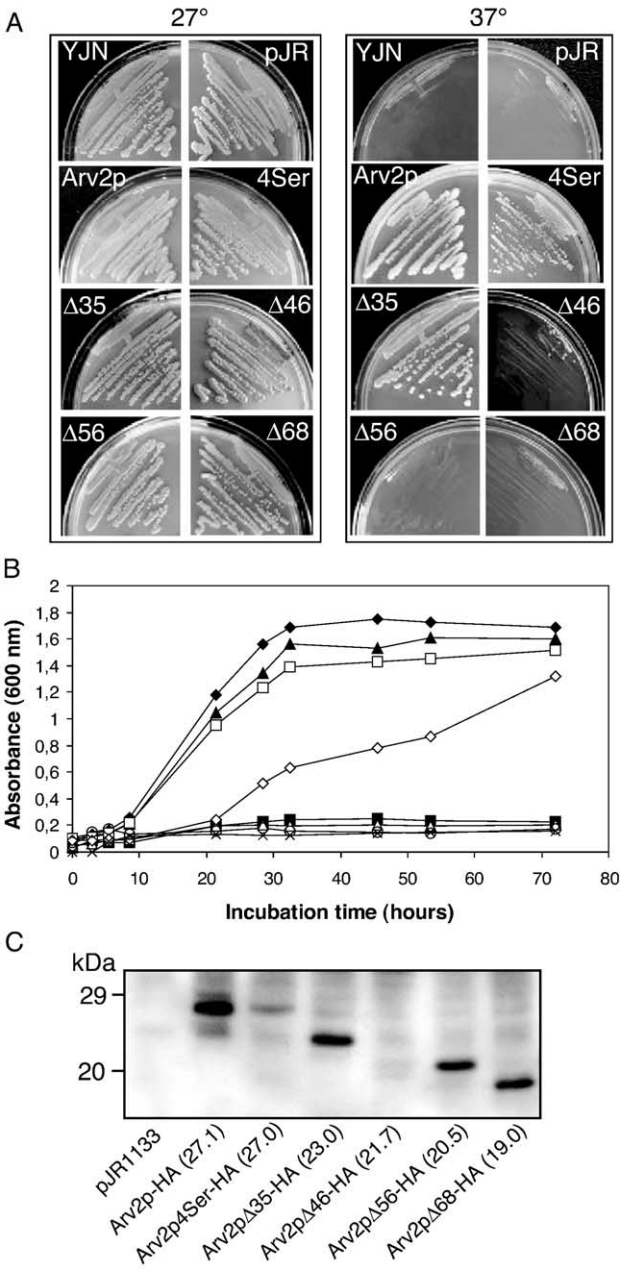

Fig. 4. Functional analysis of the NH_2-terminal region of AtArv2p. (A) Cells of the *ARV1* null mutant strain YJN1756 (YJN) and of the same strain carrying control plasmid pJR1133 (pJR) and pJR1133-derived plasmids overexpressing AtArv2p-HA (Arv2p), AtArv2p4Ser-HA (4Ser), AtArv2pΔ35-HA (Δ35), AtArv2pΔ46-HA (Δ46), AtArv2pΔ56-HA (Δ56), and AtArv2pΔ68-HA (Δ68) were streaked onto YPD plates and incubated at 27 and 37 °C for three and 2 days, respectively. (B) Single colonies of the parental wild-type strain W303-1A (♦) as well as of strain YJN1756 separately harbouring pJR1133 (■) and pJR1133-derived plasmids overexpressing AtArv2p-HA (▲), AtArv2p4-Ser-HA (◊), AtArv2pΔ35-HA (□), AtArv2pΔ46-HA (○), AtArv2pΔ56-HA (×), and AtArv2pΔ68-HA (Δ) were inoculated in minimal medium and incubated at 27 °C until OD_{600} was approximately 1.5. Cells were then diluted into YPD medium and growth at 37 °C was monitored by measuring the absorbance at 600 nm. The analysis was carried out using at least five independent colonies of each yeast strain. A representative growth curve is shown for each strain. (C) Western blot analysis of protein extracts (35 μg) from yeast cells expressing each of the HA-tagged variants of AtArv2p and from cells transformed with the control plasmid pJR1133. Immunoblots were obtained using anti-HA antibodies. The predicted size of each protein is indicated in parentheses. The positions of size markers are indicated at the left.

solid or in liquid media. Western blot analysis of extracts from the transformed cells using antibodies against the HA epitope revealed that the levels of the truncated AtArv2p-HA variants were similar to those of AtArv2p-HA with the exception of AtArv2pΔ46-HA, whose expression was barely detectable (Fig. 4C). As for the effect of disruption of the putative zinc-binding motif on AtArv2p function, cells overexpressing AtArv2p4Ser-HA also grew at 37 °C, although they formed smaller colonies on solid media and grew at a slower rate in liquid media compared with cells overexpressing AtArv2p-HA and AtArv2pΔ35-HA (Fig. 4A and B), probably because the level of AtArv2p4Ser-HA expression is clearly lower than that of AtArv2p-HA and AtArv2pΔ35-HA (Fig. 4C). Overall, these results demonstrate that the cysteine-rich subdomain of the AHD is not required for Arvp function and indicate the essential role that the C-terminal subdomain of AHD plays in Arvp activity.

3.5. Intracellular location of the A. thaliana Arv proteins

The intracellular location of AtArv proteins was investigated in onion epidermal cells co-expressing either GFP-AtArv1p or GFP-AtArv2p in combination with an ER-targeted variant of DsRed (T3RE). AtArv proteins were tagged with GFP at the amino terminus because an equivalent GFP-tagged version of yeast Arv1p has been shown to complement the growth defect of *arv1*Δ cells at 37 °C [6]. Confocal laser microscopy analysis of the transfected cells revealed in both cases a reticular pattern of green fluorescence (Fig. 5A and D) identical to the pattern of red fluorescence emitted by the T3RE protein (Fig. 5B and E). Superimposed images of GFP- and T3RE-derived fluorescence (Fig. 5C and F) confirmed that GFP-AtArv1p and GFP-AtArv2p co-localized with T3RE, thus demonstrating that both AtArv proteins are exclusively targeted to the ER membranes. A similar experiment in which a GFP-tagged version of AtArv2pΔ68 was co-expressed with T3RE revealed that a truncated AtArv2p lacking the entire AHD also localized to the ER membranes (Fig. 5G–I), thus showing that the AHD is not required for proper intracellular location of Arv proteins.

3.6. Expression analysis of the A. thaliana ARV genes

Expression of *ARV1* and *ARV2* was first analyzed by RT-PCR using pairs of primers specific for each gene and total RNA from the *A. thaliana* cell line T87, different tissues of adult plants, and 12-day-old seedlings. As a control for RNA preparations and RT-PCR conditions, we also analyzed the expression of the *A. thaliana UBQ10* gene [28]. PCR products of the expected size of 388 bp (*ARV1*) and 394 bp (*ARV2*) were amplified from all samples examined, albeit at varying levels (Fig. 6). The specificity of the amplification with each pair of primers was confirmed by restriction analysis (results not shown). To investigate in more detail the patterns of expression of *ARV1* and *ARV2*, we obtained transgenic *A. thaliana* plants carrying *ARV1::GUS* and *ARV2::GUS* genes in which fragments of 1574 and 1534 bp of the 5′-region of *ARV1* and *ARV2,* respectively, including the corresponding 5′-untranslated leader sequences and the regions coding for the first 9 (AtArv1p) and 5 (AtArv2p) amino acids, were fused in frame to the β-glucuronidase (GUS) coding sequence. Plants of several homozygous lines segregating a single T-DNA insertion for each construct were subjected to GUS histochemical analysis (Fig. 7). In floral tissues, expression of both *ARV::GUS* genes was concentrated in pollen grains (Fig. 7A and B) and fertilized ovules, which showed GUS

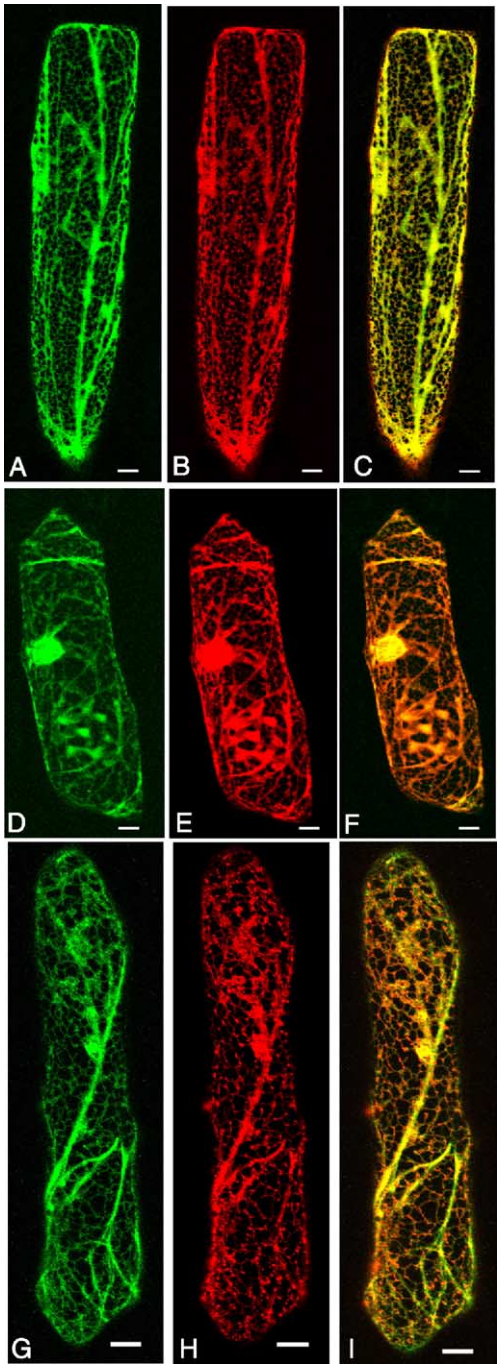

Fig. 5. Confocal laser scanning micrographs showing the distribution of fluorescence in onion epidermal cells expressing T3RE in combination with either GFP-AtArv1p (A–C), GFP-AtArv2p (D–F) or GFP-AtArv2pΔ68 (G–I). Panels show the GFP channel (A, D and G), DsRed channel (B, E and H), and merged images (C, F and I). Co-localization of GFP and T3RE fluorescence is shown in yellow. Images are three-dimensional projections of 20 sections. Scale bars = 20 μm.

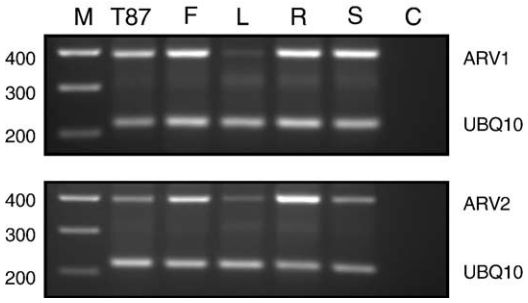

Fig. 6. RT-PCR analysis of *ARV1* and *ARV2* gene expression in *A. thaliana*. The expression of *ARV1* (top panel) and *ARV2* (bottom panel) was investigated using total RNA from *A. thaliana* suspension-cultured cells (T87), flowers (F), leaves (L), roots (R), and 12-day-old seedlings (S). PCR products were electrophoresed in a 2% agarose gel. The position of the amplified fragments corresponding to *ARV1* (388 bp), *ARV2* (394 bp), and *UBQ10* (219 bp) is indicated on the right. Lane C shows the result of RT-PCR analysis of control samples lacking RNA. Numbers on the left indicate the sizes in bp of DNA size markers shown in lane M.

staining until they developed into seeds (Fig. 7C and E). Although GUS activity was not visible in intact mature seeds, GUS expression was also detected in the internal tissues (results not shown). Occasionally, a faint blue staining was also detected in the style (Fig. 7B) whereas no staining was observed either in the remaining floral organs, including the sepals, petals, stigmatic papillae and ovary valves, or in siliques (Fig. 7A–F). Expression of *ARV1::GUS* and *ARV2::GUS* was also visible in germinating seedlings (Fig. 7K and L). However, as seedlings grew older GUS expression decreased very rapidly (Fig. 7G and H), with the exception of shoot (Fig. 7G–J) and root (Fig. 7M–P) apical meristematic regions, which retained an intense expression of both genes. Interestingly, in the shoot apical meristem the expression of *ARV2::GUS* was consistently more intense than that of *ARV1::GUS* (Fig. 7I and J). Some differences in the expression of *ARV1::GUS* and *ARV2::GUS* were also observed in the leaves. The *ARV1::GUS* gene was expressed in emerging leaves (Fig. 7I) and in the vascular tissue of adult leaves (Fig. 7Q), whereas no apparent expression of the *ARV2::GUS* gene was detected either in young emerging leaves (Fig. 7J) or in adult leaves (Fig. 7R) incubated with the GUS substrate for the same period of time. Nevertheless, some faint blue staining was observed when leaves were incubated with the GUS substrate for longer periods of time. Overall, the results shown in Fig. 7 demonstrate that *ARV1* and *ARV2* gene promoters direct largely overlapping patterns of GUS expression that are restricted to those tissues in which cells would actively divide or expand.

4. Discussion

To begin to elucidate the molecular mechanisms underlying the regulation of cellular lipid homeostasis in plants, we undertook the characterization of *A. thaliana* Arv proteins. Results presented here demonstrate that this plant contains a small *ARV* gene family of two members, *ARV1* (At1g01020) and *ARV2* (At4g01510), which encode functional AtArv1p and AtArv2p isoforms (Fig. 1) as shown by their ability to restore growth to the *S. cerevisiae ARV1* null mutant YJN1756 at 37 °C (Fig. 2). Lipid analyses demonstrated that AtArv2p

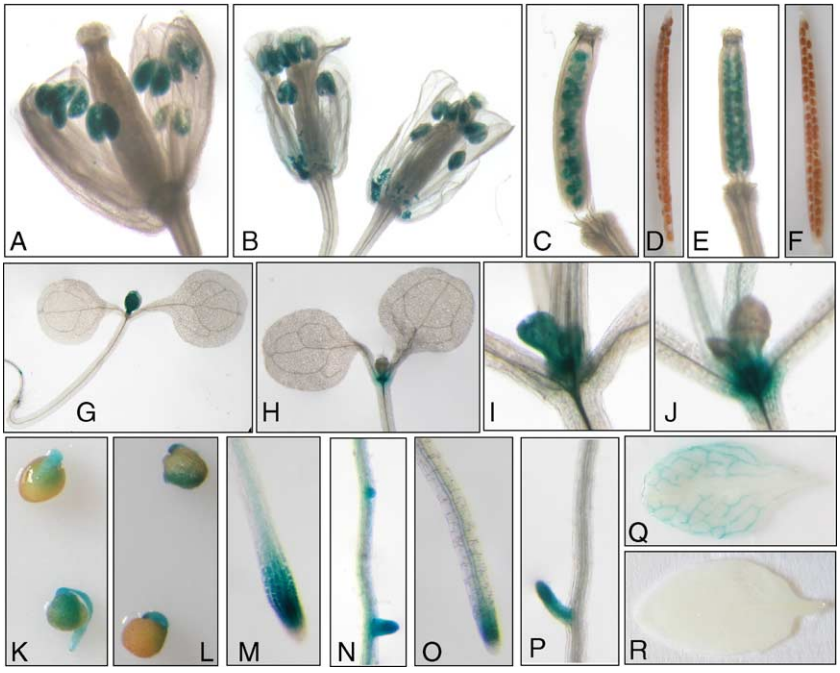

Fig. 7. Spatial and temporal patterns of expression of *ARV1* and *ARV2* genes. Histochemical analysis of GUS activity was performed in samples from *A. thaliana* plants transformed with *ARV1::GUS* (panels A, C, D, G, I, K, M, N and Q) and *ARV2::GUS* (panels B, E, F, H, J, L, O, P, R) genes. Samples were incubated at 37 °C for 16 h with the GUS substrate. The expression of GUS (indicated by blue stain) was analyzed in flowers (A and B), early-developing (C and E) and mature (D and F) siliques, 3-day-old seedlings (G and H), shoot tip of 6-day-old seedlings (I and J), seedlings 24 h after germination (K and L), primary (M and O) and lateral (N and P) root tips, and mature leaves (Q and R).

overexpression suppresses the lipid metabolic defects of *arv1*Δ cells (Fig. 3A and B). Given the high level of identity shared by AtArv1p and AtArv2p, it can be assumed that AtArv1p is also able to suppress the lipid metabolic defects of *arv1*Δ cells. This assumption is further supported by the observation that human Arv1p, which is only 33% identical to AtArv2p, also restores wild-type sterol and sphingolipid metabolism to *arv1*Δ cells [6]. Therefore, our results lead us to conclude that AtArv1p and AtArv2p are the true *A. thaliana* orthologous proteins of yeast and human Arv1p, demonstrating the universal function of Arvp in the various kingdoms of life. It is worth noting that orthologous Arv proteins appear to exist in other eukaryotic organisms such as *Schizosaccharomyces pombe* (CAC21488.1), *Caenorhabditis elegans* (CAA88728), *Danio rerio* (CB365446), *Nicotiana benthamiana* (CK284764), *Gallus gallus* (XM419587), and *Mus musculus* (NM026855).

The results of YJN1756 complementation experiments with a series of HA-tagged AtArv2p mutants (Fig. 4) revealed that the cysteine-rich subdomain of the AHD is not required for Arvp function, as growth of *arv1*Δ cells overexpressing AtArv2pΔ35-HA at 37 °C was indistinguishable from that of cells overexpressing AtArv2p-HA. The reduced capacity of AtArv2p4Ser-HA to restore the growth of *arv1*Δ cells at 37 °C does not argue against the above conclusion, as the reduction of activity correlates with a decreased expression of AtArv2p4Ser-HA compared with that of AtArv2pΔ35-HA. Hence, the apparent reduced activity of AtArv2p4Ser-HA likely stems from its low level of expression. However, the possibility that the unfolding of the putative zinc-binding motif could also alter the conformation of the adjacent C-terminal subdomain of AHD, thereby impairing the function of the protein, cannot be completely ruled out. In fact, the presence of the C-terminal subdomain of AHD appears to be essential for Arvp function, since AtArv2p activity is completely abolished when this subdomain is either partially (AtArv2pΔ56-HA) or totally (AtArv2pΔ68-HA) removed (Fig. 4). Interestingly, the loss of function of AtArv2p associated to the removal of AHD cannot be attributed to mislocalization of the truncated protein, since a GFP-tagged version of AtArv2pΔ68 is targeted to the ER membranes of onion cells, just like a GFP-tagged version of the entire AtArv2p (Fig. 5). Thus far, the biological role of the AHD subdomains remains unknown, although it has been suggested that the putative zinc-binding motif might be involved in multimerization of the protein or in mediating binding to lipid molecules [5]. Our finding that the presence of this protein motif is not required for Arvp function does not preclude the possibility that it might play an important role in the Arvp mechanism of function; for example, as a modulator of its activity. Removal of the NH_2-terminal zinc-binding motif from the *E. coli* ATPases, ClpA, ClpB, and ClpX has been reported to abolish modulation of the ATPase activity required for chaperone function, although not the chaperone activity [29]. Similarly, an allosteric regulatory role has been proposed for the zinc-binding domain of YVH1 phosphatase from *Plasmodium falciparum* [30]. As for the C-terminal moiety of AHD, no function has been suggested for this subdomain, which includes the predicted most NH_2-terminal membrane spanning sequence (residues 48 to 64) of AtArv proteins (PredictProtein) [31]. Interestingly, this specific sequence is more conserved among Arv proteins from different organisms than the remaining transmembrane sequences. These observations suggest that the C-terminal subdomain of AHD plays an essential role in Arvp mechanism of function in a capacity other than simply serving as a transmembrane sequence.

Localization experiments of GFP-tagged versions of ArArv1p and AtArv2p in onion cells demonstrated that both proteins are exclusively targeted to the ER membranes (Fig. 5), which is fully consistent not only with the prediction that AtArv1p and AtArv2p are both membrane proteins (PredictProtein) [31], but also with the observation that a fusion of GFP with *S. cerevisiae* Arv1p localizes to the ER [6]. Hence, our results show that the intracellular localization of Arvp to the ER is conserved between plants and yeast. It is, therefore, conceivable that all eukaryotic organisms might share this pattern of Arvp localization. Interestingly, as *S. cerevisiae* Arv1p also localizes to the Golgi [6], it remains to be seen whether this is a specific feature of yeast cells or, on the contrary, Arvp can also localize to the Golgi in other eukaryotic organisms.

To date nothing is known about the pattern of *ARV* gene expression in eukaryotic organisms, which prompted us to investigate the expression of *ARV1* and *ARV2* genes. A detailed expression analysis using transgenic *A. thaliana* plants carrying *ARV::GUS* chimeric genes revealed not only that both gene promoters direct largely overlapping patterns of expression (Fig. 7), as suggested by RT-PCR experiments (Fig. 6), but also that *ARV* genes have a highly specialized pattern of expression restricted to tissues in which cells are actively dividing or expanding. ARV1 and ARV2 mRNAs are also consistently detected in actively growing *A. thaliana* suspension-cultured cells (Fig. 6). These results suggest that Arvp function is important for plant cell division and expansion, which is very consistent with the proposed role of Arvp as a regulator of cellular lipid homeostasis. Actively dividing and expanding cells require a constant supply and an active intracellular transport of sterols and other lipid species to support the accompanying membrane biogenesis and to establish and maintain proper cell polarity [32,33]. For example, pollen grains contain extensive arrays of phospholipid-enriched ER membranes that are essential to sustain the dramatic increases in plasmalemma surface area that occur in the early stages of pollen tube formation [34]. A comparison of the expression pattern of the *A. thaliana ARV* genes with those of various genes coding for enzymes of the sterol biosynthetic pathway further strengthens the relationship between AtArv proteins and plant lipid metabolism. The pattern of expression of the *A. thaliana ARV* genes, particularly that of *ARV1*, is almost identical to that of the *FACKEL* gene encoding a sterol C-14 reductase implicated in the post-squalene segment of the sterol biosynthetic pathway [35]. In addition, some genes coding for enzymes of the mevalonate pathway for the production of the sterol precursor squalene are intensely expressed in tissues in which a high rate of synthesis of sterols is expected, such as pollen grains, fertilized ovules, seed tissues, and root and shoot

meristematic regions [27,36,37]. Finally, the occurrence in *A. thaliana* of two *ARV* genes showing overlapping patterns of expression and coding for highly related Arvp isoforms that share the same intracellular localization raises the question as to the physiological role of each isoform. We expect that the characterization of *A. thaliana* mutants with gain or loss of function of individual *ARV* genes will help to address this issue.

Acknowledgements

We gratefully acknowledge the technical support and facilities of the Scientific and Technical Services of the University of Barcelona. We thank Dr. Benjamin Glick from the University of Chicago for providing plasmid pDSRed.T3-N1. This work was supported by grants from the Dirección General de Investigación del Ministerio de Ciencia y Tecnología of Spain (BIO2003-1059, A.F and BMC2003-03450 to N. C.) (both grants included FEDER funds) and from the National Institutes of Health (HL67401, J.N.). O.F. and A.P. are recipients of predoctoral fellowships from the Direcció General de Recerca de la Generalitat de Catalunya. We thank Robin Rycroft for editorial assistance.

References

[1] M.K. Storey, D.M. Byers, H.W. Cook, N.D. Ridgway, Cholesterol regulates oxysterol binding protein (OSBP) phosphorylation and Golgi localization in Chinese hamster ovary cells: correlation with stimulation of sphingomyelin synthesis by 25-hydroxycholesterol, Biochem. J. 336 (1998) 247–256.

[2] A. Vik, J. Rine, Upc2p and Ecm22p, dual regulators of sterol biosynthesis in *Saccharomyces cerevisiae*, Mol. Cell. Biol. 21 (2001) 6395–6405.

[3] E. Swain, K. Baudry, J. Stukey, V. McDonough, M. Germann, J.T. Nickels, Sterol-dependent regulation of sphingolipid metabolism in *Saccharomyces cerevisiae*, J. Biol. Chem. 277 (2002) 26177–26184.

[4] T.S. Worgall, R.A. Johnson, T. Seo, H. Gierens, R.J. Deckelbaum, Unsaturated fatty acid-mediated decreases in sterol regulatory element-mediated gene transcription are linked to cellular sphingolipid metabolism, J. Biol. Chem. 277 (2002) 3878–3885.

[5] A.H. Tinkelenberg, Y. Liu, F. Alcantara, S. Khan, Z. Guo, M. Bard, L. Sturley, Mutations in yeast *ARV1* alter intracellular sterol distribution and are complemented by human *ARV1*, J. Biol. Chem. 275 (2000) 40667–40670.

[6] E. Swain, J. Stukey, V. McDonough, M. Germann, Y. Liu, S.L. Sturley, J.T. Nickels, Yeast cells lacking the *ARV1* gene harbor defects in sphingolipid metabolism, J. Biol. Chem. 277 (2002) 36152–36160.

[7] J.P. Miller, R.S. Lo, A. Ben-Hur, C. Desmarais, I. Stagljar, W. Stafford, S. Fields, Large-scale identification of yeast integral membrane protein interactions, Proc. Natl. Acad. Sci. U. S. A. 102 (2005) 12123–12128.

[8] P. Benveniste, Sterol metabolism, in: C.R. Somerville, E.M. Meyerowitz (Eds.), The Arabidopsis Book, American Society of Plant Biologists, Rockville, MD, 2002, http://www.aspb.org/publications/arabidopsis/.

[9] T.M. Dunn, D.V. Lynch, L.V. Michaelson, J.A. Napier, A post-genomic approach to understanding sphingolipid metabolism in *Arabidopsis thaliana*, Ann. Bot. 93 (2004) 483–497.

[10] M.-A. Hartmann, A.-M. Perret, J.P. Carde, C. Cassagne, P. Moreau, Inhibition of the sterol pathway in leek seedlings impairs phosphatidylserine and glucosylceramide synthesis but triggers an accumulation of triacylglycerols, Biochim. Biophys. Acta 1583 (2002) 285–296.

[11] S. Mongrand, J. Morel, J. Laroche, S. Claverol, J.-P. Carde, M.-A. Hartmann, M. Bonneu, F. Simon-Plas, R. Lessire, J.-J. Bessoule, Lipid rafts in higher plant cells: purification and characterization of TX100-insoluble microdomains from tobacco plasma membrane, J. Biol. Chem. 279 (2004) 36277–36286.

[12] G.H.H. Borner, D.J. Sherrier, T. Weimar, L.V. Michaelson, N.D. Hawkins, A. MacAskill, J.A. Napier, M.H. Beale, K.S. Lilley, P. Dupree, Analysis of detergent-resistant membranes in Arabidopsis. Evidence for plasma membrane lipid rafts, Plant Physiol. 137 (2005) 104–116.

[13] M. Bagnat, S. Keränen, A. Shevchenko, A. Shevchenko, K. Simons, Lipid rafts function in biosynthetic delivery of proteins to the cell surface in yeast, Proc. Natl. Acad. Sci. U. S. A. 97 (2000) 3254–3259.

[14] K. Simons, E. Ikonen, Functional rafts in cell membranes, Nature 387 (1997) 569–572.

[15] L.J. Pike, Lipid rafts: bringing order to the chaos, J. Lipid Res. 44 (2003) 655–667.

[16] C.R. Somerville, W.L. Ogreen, Isolation of photorespiratory mutants in *Arabidopsis*, in: M.K. Edelman, R.B. Hallick, N.H. Chua (Eds.), Methods in Chloroplast Molecular Biology, Elsevier Biomedical, New York, 1982, pp. 129–138.

[17] N. Cunillera, M. Arró, O. Forés, D. Manzano, A. Ferrer, Characterization of dehydrodolichyl diphosphate synthase of *Arabidopsis thaliana*, a key enzyme in dolichol biosynthesis, FEBS Lett. 477 (2000) 170–174.

[18] M. Rodríguez-Concepción, S. Yalovsky, M. Zik, H. Fromm, W. Gruissem, The prenylation status of a novel plant calmodulin directs plasma membrane or nuclear localization of the protein, EMBO J. 18 (1999) 1996–2007.

[19] J.A. Ortiz, J. Mallolas, C. Nicot, J. Bofarull, J.C. Rodríguez, F.G. Hegardt, D. Haro, P. Marrero, Isolation of pig mitochondrial 3-hydroxy-3-methylglutaryl-CoA synthase promoter: characterization of a peroxisome proliferator-responsive element, Biochem. J. 337 (1999) 329–335.

[20] R.D. Gietz, A. St. Jean, R.A. Woods, R.H. Schiestl, Improved method for high efficiency transformation of intact yeast cells, Nucleic Acid Res. 20 (1992) 1425.

[21] C. Mo, M. Bard, Erg28p is a key component in the yeast sterol biosynthetic enzyme complex, J. Lipid Res. 46 (2005) 1991–1998.

[22] J. Haseloff, K.R. Siemering, D.C. Prasher, S. Hodge, Removal of a cryptic intron and subcellular localization of green fluorescent protein are required to mark transgenic *Arabidopsis* plants brightly, Proc Natl. Acad. Sci. U. S. A. 94 (1997) 2122–2127.

[23] B.J. Bevis, B.S. Glick, Rapidly maturing variants of the *Discosoma* red fluorescent protein (DsRed), Nat. Biotechnol. 20 (2002) 83–87.

[24] H.R.B. Pelham, Control of protein exit from the endoplasmic reticulum, Annu. Rev. Cell Biol. 5 (1989) 1–23.

[25] W. Chiu, Y. Niwa, W. Zeng, T. Hirano, H. Kobayashi, J. Sheen, Engineered GFP as a vital reporter in plants, Curr. Biol. 6 (1996) 325–330.

[26] N. Bechtold, J. Ellis, G. Pelletier, In planta Agrobacterium-mediated gene transfer by infiltration of adult *Arabidopsis thaliana* plants, C. R. Acad. Sci. Paris/Life Sci. 316 (1993) 1194–1199.

[27] N. Cunillera, A. Boronat, A. Ferrer, Spatial and temporal patterns of GUS expression directed by 5′ regions of the *Arabidopsis thaliana* farnesyl diphosphate synthase genes FPS1 and FPS2, Plant Mol. Biol. 44 (2000) 745–758.

[28] Ch-W. Sun, J. Callis, Independent modulation of *Arabidopsis thaliana* polyubiquitin mRNAs in different organs and in response to environmental changes, Plant J. 11 (1997) 1017–1027.

[29] U.A. Wojtyra, G. Thibault, A. Tuite, W.A. Houry, The N-terminal zinc binding domain of ClpX is a dimerization domain that modulates the chaperone function, J. Biol. Chem. 278 (2003) 48981–48990.

[30] R. Kumar, A. Musiyenko, E. Cioffi, A. Oldenburg, B. Adams, V. Bitko, S. Khrisna, S. Barik, A zinc-binding dual-specificity YVH1 phosphatase in the malaria parasite, *Plasmodium falciparum*, and its interaction with the nuclear protein, pescadillo, Mol. Biochem. Parasitol. 133 (2004) 297–310.

[31] B. Rost, G. Yachdar, J. Liu, The PredictProtein server, Nucleic Acid Res. 32 (2004) W321–W326.

[32] S.D. Clouse, Arabidopsis mutants reveal multiple roles for sterols in plant development, Plant Cell 14 (2002) 1995–2000.

[33] U. Fischer, S. Men, M. Grebe, Lipid function in plant cell polarity, Curr. Opin. Plant Biol. 7 (2004) 670–676.

[34] P. Piffanelli, J.H.E. Ros, D. Murphy, Intra- and extracellular lipid composition and associated gene expression patterns during pollen development in *Brassica napus*, Plant J. 11 (1997) 549–562.
[35] J.-C. Jang, S. Fujioka, M. Tasaka, H. Seto, S. Takatsuto, A. Ishii, M. Aida, S. Yoshida, J. Sheen, A critical role of sterols in embrionyc patterning and meristem programming revealed by the *fackel* mutants of *Arabidopsis thaliana*, Genes Dev. 14 (2000) 1485–1497.
[36] M. Enjuto, V. Lumbreras, C. Marín, A. Boronat, Expression of the Arabidopsis HMG2 gene, encoding 3-hydroxy-3-methylglutaryl Coenzyme A reductase, is restricted to meristematic and floral tissues, Plant Cell 7 (1995) 517–527.
[37] M.A. Lluch, A. Masferrer, M. Arró, A. Boronat, A. Ferrer, Molecular cloning and expression analysis of the mevalonate kinase gene from *Arabidopsis thaliana*, Plant Mol. Biol. 42 (2000) 365–376.